MATERIALS CHEMISTRY FRONTIERS

RESEARCH ARTICLE

View Article Online
View Journal | View Issue

Cite this: *Mater. Chem. Front.*, 2020, **4**, 3578

Fluoro-alkyl substituted isothianaphthene bisimides as stable n-type semiconductors†

Xiaolong Chen,[a] Dongwei Zhang,[b] Yaowu He,[ac] Muhammad Umair Ali,[ad] Yuting Wu,[a] Changbin Zhao,[a] Peiheng Wu,[c] Chaoyi Yan,[a] Fred Wudl[e] and Hong Meng *[a]

The development of air-stable organic semiconductors (OSCs) with high charge mobilities is of pivotal importance for practical applications of organic thin film transistors (OTFTs) in various fields. Although several OSCs with high hole mobilities have been realized, their n-type counterparts lag far behind in terms of charge mobilities and especially air-stability potentially due to the highly sensitive nature of electrons to ambient oxidants. Isothianaphthene, a kind of non-classical thiophene, possesses a unique electronic structure and isothianaphthene bismide (BTDI) has been demonstrated as an efficient core for stable n-type OSCs. In this work, we introduced two fluoric groups with different alkyl-chains at the N-position of isothianaphthene-2,3,6,7-tetracarboxylic acid diimide and obtained new air-stable n-type OSCs, **BTDI-OCF$_3$** and **BTDI-CF**. The distinct length of the alkyl-chains caused different molecular packing styles of the resulting materials, as revealed by atomic force microscopy. The crystallinity of **BTDI-OCF$_3$** is found to be much better than **BTDI-CF** and single crystals of **BTDI-OCF$_3$** could easily be obtained by solution process. Besides, OTFTs based on these new semiconductors showed almost no hysteresis when tested in a glovebox and very small hysteresis is observed in air with a small decay of current, indicating good stability of both of these materials for their applications in n-type OTFTs.

Received 9th March 2020,
Accepted 22nd April 2020

DOI: 10.1039/d0qm00137f

rsc.li/frontiers-materials

Introduction

As an important building block for flexible and printed organic electronics, organic thin film transistors (OTFTs) have shown extensive prospects for a variety of applications, including electronic papers (e-papers), electronic skins (e-skins), sensors, radio frequency identification (RFID) tags, active-matrix displays, and synapses, owing to their large area, low cost, mechanical flexibility, and ease of fabrication.[1–5] Since the first report on OTFTs based on polythiophene in 1986,[6] intensive research efforts from both academia and industry have been dedicated to realize high performance OTFTs, leading to remarkable progress in the past few decades. For instance, a number of organic semiconductors (OSCs) have been developed with charge carrier mobilities exceeding 10 $cm^2 V^{-1} s^{-1}$ for holes and 1 $cm^2 V^{-1} s^{-1}$ for electrons.[7–11] However, the development of n-type OSCs is still far behind the p-type counterparts in terms of their carrier mobilities and especially the air-stability,[12,13] due to the high sensitivity of electrons to ambient oxidants (such as O_2 and H_2O), which seriously degrade the charge mobility and device stability of n-channel OTFTs.[14,15] On the other hand, it is noteworthy that a high-energy barrier between the active layer and the source/drain electrodes further hinders charge injection.[16] The imbalance between the characteristics of p-type and n-type semiconductors significantly restricts the practical applications of OTFTs in complementary circuits and p–n junctions.

In general, the ambient stability of n-type OSCs for applications in OTFTs could be improved through two different molecular design strategies. One is decreasing the lowest unoccupied molecular orbital (LUMO) level below than that of the most atmospheric trapping oxidants *via* introducing strong electron-withdrawing groups, such as cyano (–CN), fluoroalkyl, imide/amide and so on. It is well established that a LUMO level of *ca.* −4.0 eV or lower is beneficial to realize air-stable carrier transport for OSCs since it could minimize most

[a] *School of Advanced materials, Shenzhen Graduate School, Peking University, Shenzhen 518055, China. E-mail: menghong@pku.edu.cn*
[b] *The Institute for Solid State Physics, The University of Tokyo, 5-1-5 Kashiwanoha, Kashiwa, Chiba 277-8581, Japan*
[c] *Guangdong CNS New Material Technology Co., Ltd, Maoming 525000, China*
[d] *Department of Materials Science and Engineering, College of Engineering, Peking University, Beijing 100871, China*
[e] *Mitsubishi Chemical Center for Advanced Materials, University of California, Santa Barbara, California 93106, USA*

† Electronic supplementary information (ESI) available. CCDC 1998826. For ESI and crystallographic data in CIF or other electronic format see DOI: 10.1039/d0qm00137f

of the atmospheric trapping.[17,18] On the other hand, a low LUMO level also reduces the electron injection barrier, which allows efficient and stable electron injection and transport. Until now, a series of ambient-air-stable n-type OSCs, including perylene diimdes (PDI), naphthalene diimides (NDI), thieno[3,4-*c*]pyrrole-4,6-dione (TPD) and isoindigo have been developed.[12,19–23] Consequently, a considerable enhancement in mobility from 10^{-4} to 12.6 $cm^2\ V^{-1}\ s^{-1}$ and excellent air-stability have been realized in n-channel OTFTs.[24–26] The other approach to improve the ambient stability of n-type OSCs is promoting a more densely-packed steric barrier to the atmosphere, which could prevent moisture and oxygen penetration into the organic layer in steric.[27] The introduction of a fluoroalkyl chain to the N-atom of the NDI or PDI core could lead to dense self-segregation of the side fluoro-substituted chain, which impedes the movement of moisture and oxygen into the active channel.[28–31] More importantly, these fluoric materials not only show excellent air-stability but also exhibit high electron mobilities with considerable on/off ratios in OTFTs.[26,32–35] For instance, the highest reported electron mobility of an NDI small molecule, Cl_2-NDI, is as high as 8.6 $cm^2\ V^{-1}\ s^{-1}$ for single crystals with a slight mobility degradation of 13% (after 3 months) in ambient air.[34,36]

The electronic structure of isothianaphthene was first studied by Joseph[37] and later, Fred Wudl *et al.* reported poly(isothianaphthene) by a polymerization method.[38] The conductivity of poly(isothianaphthene) could be effectively adjusted by doping various ions. Isothianaphthene was also explored as an effective unit for low band gap conjugated polymers. In our previous work, we have reported an alkyl substituted isothianaphthene derivative, *N*,*N*′-bis(*n*-hexyl)isothianaphthene-2,3,6,7-tetracarboxylic acid diimide (**BTDI-C6**), which also possesses a deep LUMO level (−4.21 eV), approximately 0.32 eV lower than that of **NDI-C6** and much higher air-stability of the resulting OTFT devices.[39] It is well known that fluorinated substituents play a significant role in enhancing the air-stability of n-type OSCs because of their dense molecular packing, which prevents the diffusion of moisture and oxygen into the device. To date, 3-(perfluorooctyl)propyl (CF) and *p*-(trifluoromethoxy)benzyl ($BOCF_3$) substituted at the *N*,*N*′-positions of NDI have shown excellent air-stability and high mobility in OTFTs.[32,33] In this study, we introduced these two fluorinated substituents to the BTDI core to investigate their effect on the molecular packing and air-stability of the resulting BTDI derivatives, *i.e.* **BTDI-CF** and **BTDI-OCF_3**. Similar LUMO energy levels with a slight distinction of 0.02 eV were observed for these materials. Remarkably, **BTDI-CF** showed reasonable solubility in chloroform (>2 mg mL^{-1}) and **BTDI-OCF_3** also exhibited excellent solubility in chloroform (>10 mg mL^{-1}), while **NDI-OCF_3** is not soluble.[33] The OTFT devices based on **BTDI-CF** showed higher mobility (0.0368 $cm^2\ V^{-1}\ s^{-1}$) but lower air-stability than the **BTDI-OCF_3** based counterparts and both types of the devices demonstrated good air-stability with small hysteresis. The relationship between the material structure and the corresponding device performance is further studied systematically.

Experimental

Synthesis and thermal analysis

The synthetic routes of **BTDI-OCF_3** and **BTDI-CF** are shown in Scheme 1. The synthetic method was similar to that reported in the literature[39,40] and the obtained products were finally purified by sublimation with satisfactory yield. The corresponding synthetic procedures, chemical structure characterization (^{1}H NMR, ^{13}C NMR and mass spectroscopy analysis) and further experimental details are provided in the ESI.† The thermal properties of **BTDI-OCF_3** and **BTDI-CF** are characterized by thermal gravimetric analysis (TGA) and differential scanning calorimetry (DSC). **BTDI-OCF_3** showed better thermal stability and a higher melting point than **BTDI-CF** due to the more rigid substituent. Both **BTDI-OCF_3** and **BTDI-CF** exhibited good thermal stability with decomposition temperatures of up to 385 °C and 338 °C, respectively (see Fig. S1a, ESI†). In addition, the DSC results revealed melting temperatures of 264 °C and 214 °C for **BTDI-OCF_3** and **BTDI-CF**, respectively, as shown in Fig. S1b (ESI†).

Electrochemical and optical properties

The electrochemical properties of **BTDI-OCF_3** and **BTDI-CF** are studied by cyclic voltammetry (CV) in CH_2Cl_2 solution; the corresponding cyclic voltammograms are presented in Fig. 1a. As expected, both BTDI derivatives exhibited two reversible reduction peaks, indicating their typical n-type charge transfer properties. The reduction potentials of **BTDI-OCF_3** and **BTDI-CF** estimated from the onsets of the first reduction peak are

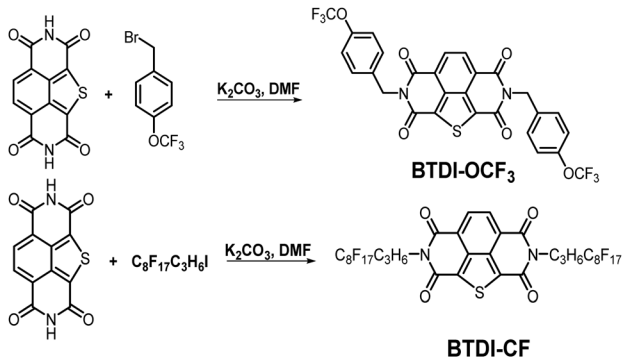

Scheme 1 The synthetic routes of **BTDI-OCF_3** and **BTDI-CF**.

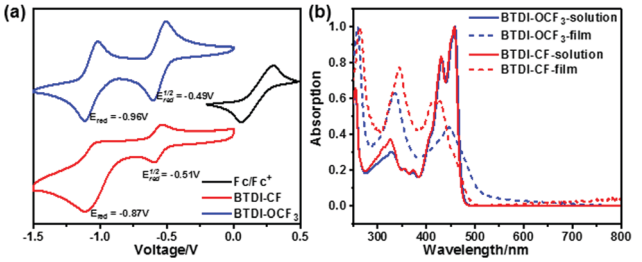

Fig. 1 (a) Cyclic voltammograms of **BTDI-CF**, **BTDI-OCF_3** and ferrocene in DCM solution. (b) UV-vis absorption spectra of the BTDI derivatives in thin films and DCM solution.

−0.49 eV and −0.51 eV, from which nearly-similar LUMO energy levels of −4.13 and −4.11 eV *versus* ferrocene were deduced. The photophysical properties of **BTDI-OCF$_3$** and **BTDI-CF** were investigated in solution and thin-film form (Fig. 1b). Similar ultraviolet (UV) absorption bands were observed for both of these compounds in dichloromethane (DCM) solution. However, the absorption spectrum of the **BTDI-OCF$_3$** thin-film showed a slight bathochromic shift with respect to **BTDI-CF**, which could be attributed to the difference in the molecular packing geometry of these materials. These results suggest that **BTDI-OCF$_3$** may exhibit stronger intermolecular interactions in the solid-state thin-film. The optical bandgap obtained from the absorption onset of thin-film spectra is estimated to be 2.43 eV for **BTDI-OCF$_3$** and 2.53 eV for **BTDI-CF**. On the other hand, density functional theory (DFT) calculations were performed at the B3LYP/6-13G(d) level by using the Gaussian 09 program package, which predicted nearly-similar LUMO levels of −4.25 eV and −4.28 eV for **BTDI-OCF$_3$** and **BTDI-CF**, respectively. Both the experimental and theoretical results revealed comparable LUMO levels of these compounds, indicating that the introduction of different fluorinated substituents at the *N*,*N*′-positions may not greatly affect the LUMO energy level of the resulting material. The corresponding electrochemical and optical properties of **BTDI-OCF$_3$** and **BTDI-CF** are summarized in Table 1.

Device fabrication and characterization

OTFTs were fabricated by thermal deposition at various substrate temperatures (T_{sub}) to optimize the device performance since T_{sub} could influence the molecular packing, grain size, grain boundaries and defects in the thin film. The device performance of OTFTs based on **BTDI-OCF$_3$** and **BTDI-CF** was tested in a glovebox; the corresponding parameters are summarized in Table 2, and the data for devices tested in air are provided in the ESI.† Both of these materials showed unique electron transfer characteristics and the **BTDI-CF** based device exhibited higher mobility than **BTDI-OCF$_3$**.

We observed that when T_{sub} is increased, the mobility of both materials is enhanced; the mobility of **BTDI-OCF$_3$** showed a slight dependence on the T_{sub}, while that of **BTDI-CF** increased 2-fold at T_{sub} = 80 °C. This will be further explained by the thin film morphological study. Interestingly, the threshold voltage (V_{th}) of the devices based on these materials showed a contrast shift trend with an increase in the T_{sub}, as can be observed from the transfer curves (Fig. 2). The $I_d^{1/2}$–V_g curves of the fabricated devices are close to linear, indicating that the mobility is independent of the gate voltage when the influence of water and oxygen is eliminated, which is ideal for logic circuits. The I_{on}/I_{off} ratios of both devices are improved since I_{off} decreased with an increase in the T_{sub}. Overall, the device performance is observed to be enhanced by elevating the T_{sub}.

Table 2 Device performance summary of the OTFTs tested in a glovebox

	T_{sub}/°C	μ_e/cm^2 V^{-1} s^{-1}	I_{on}/I_{off}	V_{th}/V
BTDI-OCF$_3$	RT[b]	6.47×10^{-3}[a] (7.05×10^{-3})[c]	10^3	−35
BTDI-OCF$_3$	60	8.94×10^{-3} (9.77×10^{-3})	10^4	−43
BTDI-OCF$_3$	90	9.21×10^{-3} (1.11×10^{-2})	10^4	−50
BTDI-CF	RT	1.50×10^{-2} (1.58×10^{-2})	10^5	−50
BTDI-CF	50	3.58×10^{-2} (3.72×10^{-2})	10^6	−33
BTDI-CF	80	3.68×10^{-2} (3.84×10^{-2})	10^7	−15

[a] Average mobility. [b] Room temperature. [c] Highest mobility.

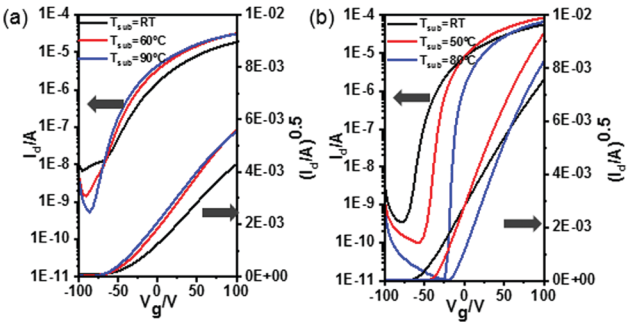

Fig. 2 Transfer characteristics of (a) **BTDI-BOCF$_3$** and (b) **BTDI-CF** based OTFTs at different T_{sub}.

The stability of the fabricated devices is investigated under different conditions. The electrical stability of the OTFTs is evaluated by a successive scan process in a glovebox. As can be seen in Fig. 3a and c, the drain–source current of **BTDI-OCF$_3$** slightly increased during the scan process, while V_{th} gradually shifted in the negative direction. This improvement in I_d could be attributed to the reduced electron trap density during constant scanning. For the **BTDI-CF** based device, after 100 cycles of scanning, the I_d–V_g curve almost remained unchanged, which showed superior stability of the device performance under N_2. This certified the remarkable operational stability of the **BTDI-CF** based device in N_2 and also indicated that the device would potentially work stably for a long time upon encapsulating it effectively. Moreover, the air-stability is also investigated by measuring the device in an ambient environment. The performance of the OTFTs tested in air initially decreased a little compared with those tested in a glovebox, illustrating that the fluoro-alkyl could protect the device against oxygen and moisture to a certain extent. However, the device performance degraded gradually with time when stored in air since oxygen and moisture could slowly diffuse into the active layer. V_{th} of both of the devices gradually shifted in the positive direction when stored in air,

Table 1 The electrochemical and optical properties of **BTDI-OCF$_3$** and **BTDI-CF**

			Experimental			Calculated				
Compound	$E_{red}^{1/2}$/V	λ_{on}/nm	E_{HOMO}/eV	E_{LUMO}/eV	Gap/eV	E_{HOMO}/eV	E_{LUMO}/eV	Gap/eV	λ_e/eV	VEA/eV
BTDI-OCF$_3$	−0.49	510.3	−6.56	−4.13	2.43	−7.03	−4.25	2.78	0.397	2.806
BTDI-CF	−0.51	489.5	−6.64	−4.11	2.53	−7.30	−4.28	3.02	0.330	2.809

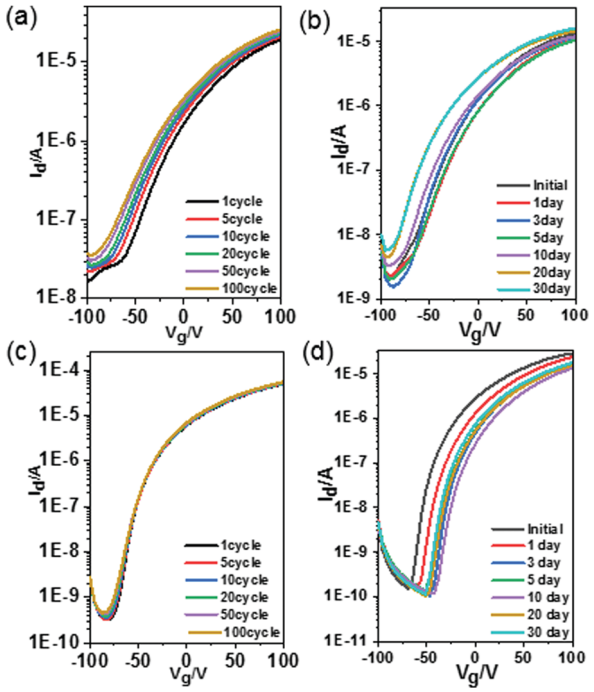

Fig. 3 Operational stability of (a) **BTDI-OCF$_3$** and (c) **BTDI-CF** based OTFTs under N_2. Transfer curves of (b) **BTDI-OCF$_3$** and (d) **BTDI-CF** based OTFTs stored and tested in air.

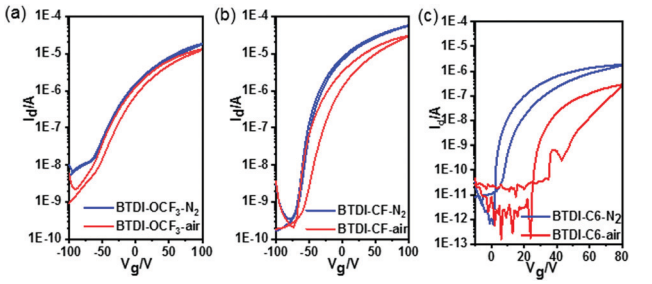

Fig. 4 Transfer characteristics of (a) **BTDI-OCF$_3$**, (b) **BTDI-CF** and (c) **BTDI-C6** based OTFTs under different testing conditions.

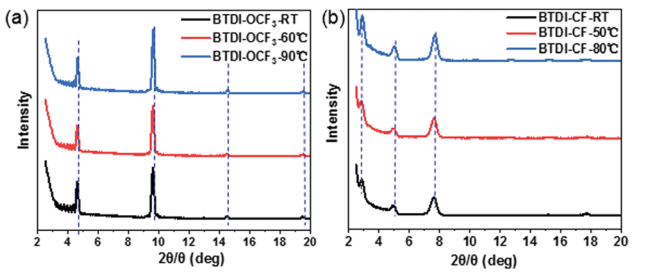

Fig. 5 XRD patterns of (a) **BTDI-OCF$_3$** and (b) **BTDI-CF** thin films deposited on OTS-treated SiO_2/Si at different T_{sub}.

which was induced by the reaction of oxygen with residual –OH in the dielectric layer.[41] Moreover, oxygen and water caused extra traps for electron transfer, which led to a drop in the mobility. The devices could still maintain n-type characteristics comparable to its initial behavior for a long time exposure to air. The scope of degradation of **BTDI-CF** was a little larger since the three methane groups (–CH_2–) negatively influenced the dense packing of the perfluorooctyl, but the device performance finally stabilized after ten days, as displayed in Table S1 (ESI†). Furthermore, OTFTs based on both **BTDI-CF** and **BTDI-OCF$_3$** exhibited almost no hysteresis when tested in N_2 and small hysteresis in air; however, the **BTDI-C6** based device showed hysteresis in N_2 and much larger hysteresis in air with a higher decay of I_{on} (Fig. 3). In general, the hysteresis is mainly caused by water and oxygen. To our knowledge, the fluroalkyl substituted BTDIs could exhibit densely packed molecular structures, which prevent water and oxygen from penetrating into the active layer, thereby reducing the hysteresis in the corresponding devices. This significant improvement in the device performance compared with our previous work[39] demonstrates that –$C_3H_6C_8F_{17}$ and *p*-(trifluoromethoxy)benzyl can kinetically protect the device performance (Fig. 4).

Structural and morphological analysis of thin films

It is widely accepted that the morphology and the microstructure of thin-films are the key factors affecting the charge mobility. To understand the mobility difference between **BTDI-CF** and **BTDI-OCF$_3$** at various T_{sub}, we analyzed the morphologies of the corresponding thin films by atomic force microscopy (AFM) and X-ray diffraction (XRD). The out-of-plane XRD patterns of BTDI thin films deposited at different T_{sub} are shown in Fig. 5. For **BTDI-OCF$_3$**, diffraction peaks up to the 4th order were observed at $2\theta = 4.6^\circ$, which correspond to (001) reflections according to the single-crystal data. The interlayer distance (*d*-spacing) estimated from the primary peak at $2\theta = 4.6^\circ$ is 1.93 nm, which is close to the unit cell vector *c*-axis of 1.97 nm obtained from single crystals. The molecular length of **BTDI-OCF$_3$** (Fig. S4, ESI†) is 2.2 nm, which is similar to the step-height of the AFM image (Fig. S5, ESI†). These results indicate that **BTDI-OCF$_3$** molecules are oriented vertically with respect to the OTS-treated SiO_2/Si substrate. Generally, this kind of molecular orientation in thin films on the substrate is beneficial for carrier transport. Besides, the intensity of the diffraction peaks exhibited a slight enhancement as the T_{sub} was increased from RT to 90 °C, indicating improved thin-film quality. This is consistent with the experimentally observed mobility of the **BTDI-OCF$_3$** based OTFTs (see Table 2). In contrast, diffraction peaks of the **BTDI-CF** thin films up to the 3rd order are clearly visible and the *d*-spacing obtained from the primary peak at $2\theta = 2.86^\circ$ is 3.07 nm, which corresponds to its longer molecular length, as evident in Fig. S4 (ESI†). Obviously, the *d*-spacing of **BTDI-CF** is larger than that of **BTDI-OCF$_3$**, which is attributed to its long fluoroalkyl chain. As expected, a slight increase in the peak intensity of the **BTDI-CF** thin films is observed after increasing the T_{sub}, which is in good agreement with the mobility observations of the **BTDI-CF** based OTFTs.

In addition, the temperature-dependent thin film morphologies of **BTDI-OCF$_3$** and **BTDI-CF** thin films were studied by AFM, as shown in Fig. 6. Among them, **BTDI-OCF$_3$** showed a well-defined terrace structure in thin-films with good crystallinity, demonstrating a remarkable improvement in the morphology

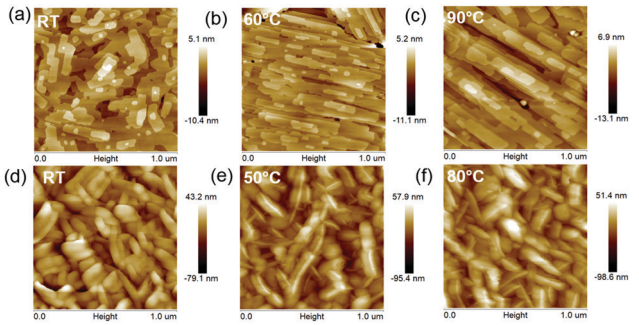

Fig. 6 AFM images of (a–c) **BTDI-OCF$_3$** and (d–f) **BTDI-CF** thin-films deposited at different T_{sub}.

upon increasing the deposition temperature. As displayed in Fig. 6a–c, the step-heights of the terraces were measured to be approximately 2.2 nm, which is in accord with the corresponding molecular length (Fig. S4, ESI†). These observations strongly support the aforementioned XRD analysis of the molecular arrangement on the substrate. Moreover, the grain size was significantly increased with increasing the T_{sub}. In general, well-defined thin-films with large grain size and good crystallinity are beneficial for efficient charge transport, suggesting that the mobility of **BTDI-OCF$_3$** based OTFTs should increase with an increase in the T_{sub}. The thin-film morphology of **BTDI-CF** was observed to be considerably different from that of **BTDI-OCF$_3$**. The **BTDI-CF** thin-film exhibited a worm-like structure with a grain size of 100–200 nm in length, as shown in Fig. 6d. In this case, T_{sub} only exhibited a slight effect on the thin-film morphology. As depicted in Fig. 6e, the grain size was slightly increased after increasing the T_{sub} from RT to 50 °C. However, the film morphology hardly changed after continuously raising T_{sub} (Fig. 6f), indicating that the device performance would remain unchanged at higher deposition temperatures. As expected, the above investigations are consistent with the observed mobility tendency of **BTDI-OCF$_3$** and **BTDI-CF** based OTFTs, as summarized in Table 2.

Conclusions

In summary, we have successfully synthesized two kinds of fluoro-alkyl substituted isothianaphthene materials, **BTDI-OCF$_3$** and **BTDI-CF**. Both of these BTDI derivatives have similar LUMO energy levels and optical properties since the substituent on the nitrogen atom does not greatly affect the LUMO energy. However, the molecular packing and thin film morphologies are quite different due to the significant difference of the alkyl-chain lengths. This further influenced the device performance; the **BTDI-CF** based OTFT showed higher mobility (0.0368 $cm^2 V^{-1} s^{-1}$) with excellent operational stability in a glovebox, while the **BTDI-OCF$_3$** based device demonstrated highly ordered molecular packing, which resulted in enhanced air-stability. Notably, the hysteresis phenomenon and current decay tested in air compared with those under N_2 of the OTFTs based on both of these materials exhibited great improvement as compared to the BTDI-C6 reported in our previous work, indicating better stability of these newly developed fluoric BTDI derivatives. Moreover, the solubility of these compounds is much higher than the NDI analogues with the same substituent. Further investigation of solution processing of OTFTs based on these materials is underway in our lab.

Conflicts of interest

There are no conflicts to declare.

Acknowledgements

This work was financially supported by Shenzhen Science and Technology Research Grant (JCYJ20170412151139619, JCYJ20190808175216899 and JCYJ20190808182803805), Key-Area Research and Development Program of Guangdong Province (2019B010924003), NSFC-RS International Exchanges Programme (5181102182), Natural Science Foundation of Guangdong Province (2020A1515010449), Special Foundation for Science and Technology of Guangdong Province (2020S0007), and Guangdong Academician Expert Enterprise Workstation of Guangdong CNS New Material Technology Co., Ltd.

Notes and references

1 A. F. Paterson, S. Singh, K. J. Fallon, T. Hodsden, Y. Han, B. C. Schroeder, H. Bronstein, M. Heeney, I. McCulloch and T. D. Anthopoulos, Recent Progress in High-Mobility Organic Transistors: A Reality Check, *Adv. Mater.*, 2018, **30**, 1801079.
2 J. Yang, Z. Zhao, S. Wang, Y. Guo and Y. Liu, Insight into High-Performance Conjugated Polymers for Organic Field-Effect Transistors, *Chem*, 2018, **4**, 2748–2785.
3 A. C. Arias, J. D. MacKenzie, I. McCulloch, J. Rivnay and A. Salleo, Materials and applications for large area electronics: Solution-based approaches, *Chem. Rev.*, 2010, **110**, 3–24.
4 C. Wang, H. Dong, W. Hu, Y. Liu and D. Zhu, Semiconducting π-conjugated systems in field-effect transistors: A material odyssey of organic electronics, *Chem. Rev.*, 2012, **112**, 2208–2267.
5 Z. Lv, Y. Zhou, S. Han and V. A. L. Roy, From biomaterial-based data storage to bio-inspired artificial synapse, *Mater. Today*, 2018, **21**, 537–552.
6 A. Tsumura, H. Koezuka and T. Ando, Macromolecular electronic device: Field-effect transistor with a polythiophene thin film, *Appl. Phys. Lett.*, 1986, **49**, 1210–1212.
7 H. Minemawari, T. Yamada, H. Matsui, J. Y. Tsutsumi, S. Haas, R. Chiba, R. Kumai and T. Hasegawa, Inkjet printing of single-crystal films, *Nature*, 2011, **475**, 364–367.
8 I. Vladimirov, M. Kellermeier, T. Geßner, Z. Molla, S. Grigorian, U. Pietsch, L. S. Schaffroth, M. Kühn, F. May and R. T. Weitz, High-mobility, ultrathin organic semiconducting films realized by surface-mediated crystallization, *Nano Lett.*, 2018, **18**, 9–14.
9 G. Schweicher, V. Lemaur, C. Niebel, C. Ruzié, Y. Diao, O. Goto, W.-Y. Lee, Y. Kim, J. B. Arlin, J. Karpinska, A. R. Kennedy, S. R. Parkin, Y. Olivier, S. C. B. Mannsfeld, J. Cornil, Y. H. Geerts and Z. Bao, Bulky end-capped [1]benzothieno[3,2-*b*]benzothiophenes: Reaching high-mobility organic semiconductors by fine

tuning of the crystalline solid-state order, *Adv. Mater.*, 2015, **27**, 3066–3072.
10 Y. Xiong, J. Tao, R. Wang, X. Qiao, X. Yang, D. Wang, H. Wu and H. Li, A Furan–Thiophene-Based Quinoidal Compound: A New Class of Solution-Processable High-Performance n-Type Organic Semiconductor, *Adv. Mater.*, 2016, **28**, 5949–5953.
11 H. R. Tseng, H. Phan, C. Luo, M. Wang, L. A. Perez, S. N. Patel, L. Ying, E. J. Kramer, N. Thuc-Quyen, G. C. Bazan and A. J. Heeger, High-mobility field-effect transistors fabricated with macroscopic aligned semiconducting polymers, *Adv. Mater.*, 2014, **26**, 2993–2998.
12 J. Dhar, U. Salzner and S. Patil, Trends in molecular design strategies for ambient stable n-channel organic field effect transistors, *J. Mater. Chem. C*, 2017, **5**, 7404–7430.
13 X. Gao and Y. Hu, Development of n-type organic semiconductors for thin film transistors: A viewpoint of molecular design, *J. Mater. Chem. C*, 2014, **2**, 3099–3117.
14 A. R. Murphy and J. M. J. Fréchet, Organic semiconducting oligomers for use in thin film transistors, *Chem. Rev.*, 2007, **107**, 1066–1096.
15 L. L. Chua, J. Zaumseil, J. F. Chang, E. C. W. Ou, P. K. H. Ho, H. Sirringhaus and R. H. Friend, General observation of n-type field-effect behaviour in organic semiconductors, *Nature*, 2005, **434**, 194.
16 G. R. Hutchison, M. A. Ratner and T. J. Marks, Intermolecular charge transfer between heterocyclic oligomers. Effects of heteroatom and molecular packing on hopping transport in organic semiconductors, *J. Am. Chem. Soc.*, 2005, **127**, 16866–16881.
17 Y. Chang, M. Kuo, C. Chen, H. Lu and I. Chao, On the air stability of n-channel organic field-effect transistors: A theoretical study of adiabatic electron affinities of organic semiconductors, *J. Mater. Chem. C*, 2010, **114**, 11595–11601.
18 H. Usta, C. Risko, Z. Wang, H. Huang, M. K. Deliomeroglu, A. Zhukhovitskiy, A. Facchetti and T. J. Marks, Design, synthesis, and characterization of ladder-type molecules and polymers. Air-stable, solution-processable n-channel and ambipolar semiconductors for thin-film transistors via experiment and theory, *J. Am. Chem. Soc.*, 2009, **131**, 5586–5608.
19 H. E. Katz, A. J. Lovinger, J. Johnson, C. Kloc, T. Siegrist, W. Li, Y. Y. Lin and A. Dodabalapur, A soluble and air-stable organic semiconductor with high electron mobility, *Nature*, 2000, **404**, 478.
20 X. Guo, A. Facchetti and T. J. Marks, Imide- and amide-functionalized polymer semiconductors, *Chem. Rev.*, 2014, **114**, 8943–9021.
21 J. D. Yuen, V. A. Pozdin, A. T. Young, B. L. Turner, I. D. Giles, J. Naciri, S. A. Trammell, P. T. Charles, D. A. Stenger and M. A. Daniele, Perylene-diimide-based n-type semiconductors with enhanced air and temperature stable photoconductor and transistor properties, *Dyes Pigm.*, 2020, **174**, 108014.
22 O. A. Melville, T. M. Grant and B. H. Lessard, Silicon phthalocyanines as N-type semiconductors in organic thin film transistors, *J. Mater. Chem. C*, 2018, **6**, 5482–5488.
23 S. M. Swick, T. Gebraad, L. Jones, B. Fu, T. J. Aldrich, K. L. Kohlstedt, G. C. Schatz, A. Facchetti and T. J. Marks, Building Blocks for High-Efficiency Organic Photovoltaics: Interplay of Molecular, Crystal, and Electronic Properties in Post-Fullerene ITIC Ensembles, *ChemPhysChem*, 2019, **20**, 2608–2626.
24 C. Zhang, Y. Zang, E. Gann, C. R. McNeill, X. Zhu, C.-A. Di and D. Zhu, Two-dimensional π-expanded quinoidal terthiophenes terminated with dicyanomethylenes as n-type semiconductors for high-performance organic thin-film transistors, *J. Am. Chem. Soc.*, 2014, **136**, 16176–16184.
25 J. Dou, Y. Zheng, Z. Yao, Z. Yu, T. Lei, X. Shen, X. Luo, J. Sun, S. Zhang, Y. Ding, G. Han, Y. Yi, J. Wang and J. Pei, Fine-tuning of crystal packing and charge transport properties of BDOPV derivatives through fluorine substitution, *J. Am. Chem. Soc.*, 2015, **137**, 15947–15956.
26 N. A. Minder, S. Ono, Z. Chen, A. Facchetti and A. F. Morpurgo, Band-Like Electron Transport in Organic Transistors and Implication of the Molecular Structure for Performance Optimization, *Adv. Mater.*, 2012, **24**, 503–508.
27 B. A. Jones, A. Facchetti, M. R. Wasielewski and T. J. Marks, Tuning orbital energetics in arylene diimide semiconductors. Materials design for ambient stability of n-type charge transport, *J. Am. Chem. Soc.*, 2007, **129**, 15259–15278.
28 H. E. Katz, A. J. Lovinger, J. Johnson, C. Kloc, T. Siegrist, W. Li, Y. Y. Lin and A. Dodabalapur, A soluble and air-stable organic semiconductor with high electron mobility, *Nature*, 2000, **404**, 478–481.
29 R. Schmidt, J. H. Oh, Y.-S. Sun, M. Deppisch, A.-M. Krause, K. Radacki, H. Braunschweig, M. Könemann, P. Erk, Z. Bao and F. Würthner, High-performance air-stable n-channel organic thin film transistors based on halogenated perylene bisimide semiconductors, *J. Am. Chem. Soc.*, 2009, **131**, 6215–6228.
30 B. J. Jung, J. Sun, T. Lee, A. Sarjeant and H. E. Katz, Low-temperature-processible, transparent, and air-operable n-channel fluorinated phenylethylated naphthalenetetracarboxylic diimide semiconductors applied to flexible transistors, *Chem. Mater.*, 2009, **21**, 94–101.
31 K. C. See, C. Landis, A. Sarjeant and H. E. Katz, Easily synthesized naphthalene tetracarboxylic diimide semiconductors with high electron mobility in air, *Chem. Mater.*, 2008, **20**, 3609–3616.
32 B. J. Jung, K. Lee, J. Sun, A. G. Andreou and H. E. Katz, Air-Operable, High-Mobility Organic Transistors with Semifluorinated Side Chains and Unsubstituted Naphthalenetetracarboxylic Diimide Cores: High Mobility and Environmental and Bias Stress Stability from the Perfluorooctylpropyl Side Chain, *Adv. Funct. Mater.*, 2010, **20**, 2930–2944.
33 D. Zhang, L. Zhao, Y. Zhu, A. Li, C. He, H. Yu, Y. He, C. Yan, O. Goto and H. Meng, Effects of p-(trifluoromethoxy)benzyl and p-(trifluoromethoxy)phenyl molecular architecture on the performance of naphthalene tetracarboxylic diimide-based air-stable n-type semiconductors, *ACS Appl. Mater. Interfaces*, 2016, **8**, 18277–18283.
34 T. He, M. Stolte, C. Burschka, N. H. Hansen, T. Musiol, D. Kälblein, J. Pflaum, X. Tao, J. Brill and F. Würthner,

Single-crystal field-effect transistors of new Cl_2-NDI polymorph processed by sublimation in air, *Nat. Commun.*, 2015, **6**, 5954.

35 C. Liu, C. Xiao, Y. Li, W. Hu, Z. Li and Z. Wang, High performance, air stable n-type single crystal transistors based on core-tetrachlorinated perylene diimides, *Chem. Commun.*, 2014, **50**, 12462–12464.

36 T. He, M. Stolte and F. Wuerthner, Air-Stable n-Channel Organic Single Crystal Field-Effect Transistors Based on Microribbons of Core-Chlorinated Naphthalene Diimide, *Adv. Mater.*, 2013, **25**, 6951–6955.

37 J. D. Heer, The electronic structure of conjugated sulfur compounds. I. Thiophene and isothianaphthene, *J. Am. Chem. Soc.*, 1954, **76**, 4802–4806.

38 F. Wudl, M. Kobayashi and A. J. Heeger, Poly(isothianaphthene), *J. Org. Chem.*, 1984, **49**, 3382–3384.

39 X. Chen, Y. He, M. U. Ali, Y. He, Y. Zhu, A. Li, C. Zhao, I. F. Perepichka and H. Meng, Isothianaphthene diimide: an air-stable n-type semiconductor, *Sci. China: Chem.*, 2019, **62**, 1360–1364.

40 C. P. Yu, R. Kimura, T. Kurosawa, E. Fukuzaki, T. Watanabe, H. Ishii, S. Kumagai, M. Yano, J. Takeya and T. Okamoto, Air-Stable Benzo[c]thiophene Diimide n-Type π-Electron Core, *Org. Lett.*, 2019, **21**, 4448–4453.

41 D. Kumaki, T. Umeda and S. Tokito, Influence of H_2O and O_2 on threshold voltage shift in organic thin-film transistors: Deprotonation of SiOH on SiO_2 gate-insulator surface, *Appl. Phys. Lett.*, 2008, **92**, 093309.

